Portrayal of the Color Polymorphism in the 5-Acetyl-derivative of ROY

Bernardo A. Nogueira,[*,1] Maria Carvalho,[1] José A. Paixão,[2] M. Ermelinda S. Eusébio,[1]

Susana M. M. Lopes,[1] Teresa M. V. D. Pinho e Melo[1] and Rui Fausto[1]

[1] *University of Coimbra, CQC-IMS, Department of Chemistry, P-3004-535 Coimbra, Portugal.*
[2] *University of Coimbra, CFisUC, Department of Physics, P-3004-516 Coimbra, Portugal.*

Abstract

A novel derivative of the prominent ROY compound, 5-acetyl-2-((2-nitrophenyl)amino)thiophene-3-carbonitrile (AcROY), was synthesized in a two-steps procedure by the nucleophilic aromatic substitution reaction between 1-fluoro-2-nitrobenzene and 2-aminothiophene-3-carbonitrile, followed by Friedel–Crafts acylation at position 5 of the thiophene ring. The conformational space of the compound (isolated molecule) was studied computationally, rendering 4 low-energy intramolecularly hydrogen-bonded conformers. The compound exhibits color polymorphism, with 3 different polymorphs identified. The crystal structures of two of the polymorphs were solved by single-crystal X-ray diffraction crystallography: polymorph **1** (burgundy) is monoclinic ($P2_1/n$; a = 5.3354(2) Å, b = 14.2344(4) Å, c = 17.1709(6) Å, β = 96.567(2)º, Z = 4, Z' = 1), and polymorph **2** (orange) is monoclinic ($P2_1/c$; a = 25.451(3) Å, b = 14.4966(14) Å, c = 7.1113(7) Å, β = 95.795(6)º, Z = 8, Z' = 2. It was not possible to determine the crystal structure of the third polymorph (**3**, orange-yellowish), but the obtained powder X-ray diffraction, infrared and Raman spectroscopy data clearly demonstrate the existence of this additional polymorphic form. Indexation of its powder diffraction pattern showed that it is a monoclinic variety with lattice parameters a = 11.383(3) Å, b = 13.6609(3) Å, c = 25.247(7) Å, β =101.75(1), thus exhibiting a more complex supramolecular structure compared to polymorphs **1** and **2**. All polymorphs were characterized spectroscopically (by infrared and Raman spectroscopies) and by thermal analysis (by differential scanning calorimetry and polarized light thermomicroscopy). Interestingly, among the 4 predicted low energy conformers of the AcROY molecule, only the most stable form was found to be present in the crystals of the two structurally characterized polymorphs of the compound. The dominant intermolecular interactions in polymorphs **1** and **2** were investigated (also using Hirshfeld surface analysis) and were found to be significantly different. The observed polymorphism of AcROY is then an interesting case of packing-determined color polymorphism.

Keywords: 5-acetyl-2-((2-nitrophenyl)amino)thiophene-3-carbonitrile, ROY, color polymorphism, molecular structure, crystal structure, thermal analysis, infrared, Raman and NMR spectroscopies.

* Corresponding author e-mail: ban@qui.uc.pt

Introduction

5-Methyl-2-((2-nitrophenyl)amino)-3-thiophenecarbonitrile, better known as ROY due to the red, orange and yellow colors of its different crystalline varieties, is the most polymorphic organic material on record, with thirteen polymorphs already described.[1–6] Interestingly, most of these differently colored polymorphs owe their chromaticity diversity to the different molecular conformations assumed by the molecules in the crystals.[7] The ROY molecule comprises two essentially rigid fragments (nitrophenyl and methyl-thiophenecarbonitrile) connected by an amine bridge (Scheme 1). The soft potential for internal rotation around the N–C bond connecting the substituted thiophene ring to the bridge provides the molecule a rich conformational landscape, which can be easily affected by intermolecular interactions in crystalline phase.[1-7] When the two rings of the molecule are nearly co-planar (*i.e.*, when the dihedral angle θ in Scheme 1 is closer to 180º or 0º), ROY crystals tend to be reddish, due to the large π electron conjugation taking place in these cases. On the other hand, when the θ dihedral is close to 90º, the two rings became nearly perpendicular, thus reducing the extent of the π electron conjugation, and the crystals have the propensity to present yellow tones. The orange colors are mostly exhibited by crystals where this dihedral angle assumes intermediate values.[6–8] Nevertheless, at least two polymorphs of ROY have been shown to present remarkably different colors despite the conformation of their constituting molecules being nearly identical,[9] indicating that dissimilar intermolecular forces *per se* can give rise to polymorphs of ROY showing notoriously diverse colors. As it has been recognized,[7] ROY is in fact a comprehensive case of a compound exhibiting both conformational and packing color polymorphisms.

In the continuation of our recent investigations in systems exhibiting color polymorphism,[7,10] in this article we report the results of our studies on a novel compound belonging to the ROY family that also exhibits color polymorphism: 5-acetyl-2-((2-nitrophenyl)amino)thiophene-3-carbonitrile (from now on designated as AcROY). The newly synthesized compound differs from ROY by replacement of the methyl substituent present in the thiophene ring of ROY by an acetyl group (see Scheme 1). The study included the structural and conformational characterization of the isolated molecule of the compound using density functional theory (DFT) calculations, as well as the synthesis of the compound, screening of its polymorphs, and their characterization using X-ray diffraction, infrared (IR) and Raman spectroscopies, differential scanning calorimetry (DSC), and polarized light thermal microscopy (PLTM). Our main motivation for studying this chemical system resulted from the fact that there are not many examples of ROY-related compounds described in the literature,[6,11–14] in spite of the appealing properties of this type of compounds. By including the conformationally flexible acetyl substituent in the molecule (instead of the methyl group present in ROY), our general goal was to contribute to the understanding of how modifications in the basic ROY structure impact polymorphism, with emphasis on the mechanisms responsible for the different colors of the polymorphs. As described in details below, and according to our expectations, AcROY was found to

exhibit 3 different polymorphs of different colors: **1**, burgundy; **2**, orange; **3**, orange-yellowish. The crystal structure of polymorphs **1** and **2** could be determined by single crystal X-ray crystallography, and all polymorphs were characterized spectroscopically (IR, Raman) and by thermal analysis (DSC/PLTM). Interestingly, among the 4 predicted low energy conformers of the molecule, only the most stable form was found to be present in the crystals of the two structurally characterized polymorphs of the compound. On the other hand, polymorph **1** has a single independent molecule per crystal unit cell (*Z'* = 1) and 4 molecules in the cell (*Z* = 4), while in polymorph **2** *Z'* = 2 and *Z* = 8, and the dominant intermolecular interactions were found to be substantially different in the two polymorphs (as noticed also in the performed Hirshfeld analysis of the two crystalline structures). The observed polymorphism of AcROY is then an interesting case of packing-determined color polymorphism.

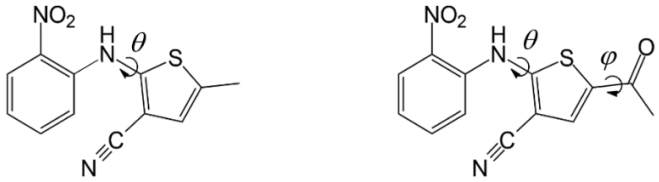

Scheme 1 – Molecular structures of ROY *(left*) and AcROY(*right*), with indication of the conformationally relevant internal rotations (*θ, φ*). In all low energy conformers of the two molecules, the nitrophenyl fragment is kept nearly co-planar with the NH bridging bond and oriented as depicted, due to the presence of a stabilizing intramolecular N–H···O hydrogen bond that blocks the conformational flexibility around the C–N bond connecting these two fragments.[1-10]

Below, the presentation of the results is organized in the following manner: *(i)* first, the synthesis of the compound is described and its general characterization provided; *(ii)* then, the structure of the isolated molecule of the compound, preferred conformations and their relative energies and barriers of interconversion are presented, and the major intramolecular interactions determining the structural and energetic features of the molecule of AcROY are discussed; these results provide the basis for the subsequent structural analysis of the polymorphs and effects of intermolecular interactions on the intramolecular potentials and structure of individual molecules in the crystals; *(iii)* the polymorph screening experiments are then presented; these were done using optical microscopy and Raman and infrared spectroscopies; *(iv)* following the spectroscopic identification of the three different polymorphs, X-ray diffraction data is presented for detailed structural characterization of polymorphs **1** and **2**, for which suitable crystals for single crystal experiments were obtained, and a general characterization of the unit cell of polymorph **3**, by X-ray powder diffraction, is provided; for polymorphs **1** and **2**, intermolecular interactions present in the crystals are analyzed in details by means of Hirshfeld analysis; *(v)* finally, the thermal analysis of the polymorphs is presented, which includes DSC, PLTM and temperature variation Raman spectroscopy studies.

Materials and Methods

Synthesis and polymorphs screening

General information: AcROY was synthesized in a two-step procedure by the nucleophilic aromatic substitution reaction between 1-fluoro-2-nitrobenzene (**I**) and 2-aminothiophene-3-carbonitrile (**II**) followed by Friedel–Crafts acylation at position 5 of the thiophene ring, as outlined in Scheme 2. The reaction of 1-fluoro-2-nitrobenzene (**I**) with 2-aminothiophene-3-carbonitrile (**II**) gave compound **III** in high yield (76%). Zinc chloride-catalyzed Friedel–Crafts acylation of compound **III**, using acetic anhydride as the acylating agent, afforded the target AcROY in 83% yield. The reagents and solvents were obtained commercially analytical grade.

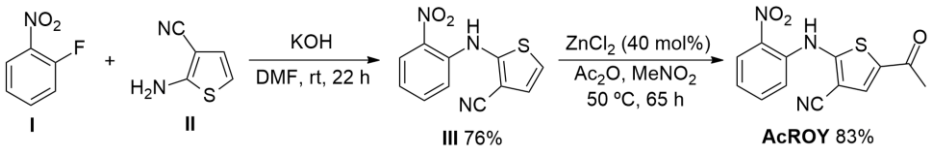

Scheme 2 – Synthetic route to AcROY.

*Synthesis of 2-((2-nitrophenyl)amino)thiophene-3-carbonitrile (**III**)*: a solution of 2-aminothiophene-3-carbonitrile (10 mmol, 1.24 g) and 1-fluoro-2-nitrobenzene (10 mmol, 1.05 mL) in dimethylformamide (15 mL) were added dropwise to a suspension of KOH (15 mmol, 0.842 g) in dimethylformamide (2.5 mL). After the addition was complete, the reaction mixture was stirred at room temperature for 6 h and an additional portion of KOH (5 mmol, 0.281 g) was added at once, and the reaction mixture was stirred for another 16 h. The reaction mixture was poured into a mixture of water/ice and extracted with dichloromethane (3 x 20 mL). The combined organic phases were washed with HCl 1M (2 x 30 mL) and brine (2 x 20 mL), dried and the solvent evaporated off. The compound was obtained as a red solid (7.59 mmol, 76%) by crystallization from ethanol, filtered and dried under vacuum. mp 129.5-131.0 ºC (from ethanol). IR (ATR) ν 710, 735, 771, 814, 841, 879, 947, 969, 1053, 1068, 1093, 1146, 1217, 1235, 1275, 1319, 1344, 1378, 1403, 1440, 1456, 1501, 1549, 1589, 1610, 2211, 3106, 3167, 3204 cm^{-1}. ^{1}H NMR δ ($CDCl_3$): 7.01 (ddd, *J* = 8.4, 7.2 and 1.2 Hz, 1H), 7.10 (d, *J* = 6.0 Hz, 1H), 7.14 (d, *J* = 6.0 Hz, 1H), 7.28 (dd, *J* = 8.8 and 1.2 Hz, 1H), 7.53-7.57 (m, 1H), 8.27 (dd, *J* = 8.4 and 1.6 Hz, 1H), 9.80 (s, 1H). ^{13}C NMR δ ($CDCl_3$): 104.0, 113.6, 116.2, 120.4, 120.7, 126.8, 126.9, 134.5, 136.3, 140.6, 151.7. HRMS (ESI) *m/z* for $C_{11}H_8N_3O_2S$ [M + H^+] calcd. 246.0332, found 246.0329.

Synthesis of 5-acetyl-2-((2-nitrophenyl)amino)thiophene-3-carbonitrile (AcROY): zinc chloride anhydrous (40 mol%, 1.30 mmol, 0.18 g) and acetic anhydride (8.15 mL) were added to a solution of compound **III** (3.26 mmol, 0.80 g) in nitromethane (16.3 mL). The reaction mixture was stirred in a bath at 50 ºC for 65 h. After this time, the reaction was allowed to cool to room temperature and dichloromethane (30 mL) and saturated aqueous $NaHCO_3$ (50 mL) were added. The phases were separated, the organic phase

was washed with saturated aqueous $NaHCO_3$ (2 x 50 mL), dried and the solvent evaporated off. AcROY was obtained as an orange solid (2.71 mmol, 83%) by crystallization from ethanol, filtered and dried under vacuum. mp 181.7-183.0 ºC (from ethanol). IR (ATR) ν 708, 744, 761, 775, 787, 847, 856, 878, 1021, 1146, 1162, 1214, 1257, 1318, 1359, 1455, 1494, 1527, 1546, 1582, 1665, 1721, 2213, 2969, 3150, 3232 cm^{-1}. ^1H NMR δ ($CDCl_3$): 2.53 (s, 3H), 7.21 (ddd, *J* = 8.4, 7.2 and 1.2 Hz, 1H), 7.63 (s, 1H), 7.67-7.74 (m, 1H), 7.79 (dd, *J* = 8.4 and 1.2 Hz, 1H), 8.34 (dd, *J* = 8.5 and 1.5 Hz, 1H), 10.78 (s, 1H). ^{13}C NMR δ ($CDCl_3$): 25.7, 97.1, 113.0, 117.5, 122.9, 127.2, 131.9, 132.9, 136.0, 136.4, 136.5, 159.4, 189.4. HRMS (ESI) *m*/*z* for $C_{13}H_{10}N_3O_3S$ [M + H^+] calcd. 288.0437, found 288.0434.

Polymorphs screening: the different polymorphs of AcROY were obtained by slow evaporation recrystallization from different solvent solutions, at room temperature. The solutions were prepared by dissolving 10-30 mg of AcROY in 5-20 mL of solvent. All solutions were filtered to prevent the crystallization from crystalline seeds that were not possible to solubilize.

Instrumental methods

For the initial characterization of the synthesized compounds, the ^1H and ^{13}C NMR spectra (Figures S1 and S2 in the Supporting Information) were recorded on a Bruker Avance III instrument, operating at 400 MHz and at 100 MHz, respectively. The solvent used was deuterochloroform ($CDCl_3$). High-resolution mass spectroscopy (HRMS) was performed by electrospray ionization (ESI) on an orbitrap q-exactive focus mass spectrometer. Melting point (uncorrected) was determined in an open glass capillary. Thin-layer chromatography (TLC) analyses were performed using precoated silica gel plates.

The Raman spectra were obtained using a micro-Raman Horiba LabRam HR Evolution system, with excitation provided by a 532 nm solid-state laser, using an approximate power of 0.5 mW at the sample, to prevent photodegradation of the compound. A 50× long working distance objective was used, with a laser spot diameter of around 1 μm in the sample. The equipment was calibrated using a Si crystal (reference band at 520.5 cm^{-1}). The final spectra were the average of 100-500 accumulations of spectra obtained with an acquisition-time of 0.5-1.0 s and resolution of 0.5 cm^{-1}. For the temperature variation Raman experiments, a hot stage THMS 600 (Linkam Scientific Instruments), controlled by a T95-PE Linkpad controlling unit, was used.

The infrared spectra were collected in the attenuated total reflectance (ATR) mode, on a Thermo Scientific FT-IR Nicolet iS5 system, with an iD7 ATR accessory (angle of incidence: 45º; crystal: diamond). The spectra were recorded with spectral resolution of 1 cm^{-1}, in the wavenumber range of 400–4000 cm^{-1}, being the average of 512 scans.

The single crystal X-ray diffraction experiments were performed at room temperature using graphite monochromated MoKα (λ = 0.71073 Å) radiation in a Bruker APEX II diffractometer. The structures were solved by the dual-space algorithm implemented in SHELXT-2018/2,[15] and full-matrix least-squares

refinement of the structural models were performed using SHELXL-2018/3.[16] All non-hydrogen atoms were refined anisotropically. Hydrogen atoms were placed at calculated idealized positions and refined as riding using SHELXL-2018/3 default values,[16] except for those of the amine groups that were refined isotropically with a displacement parameter constrained to 1.2× the U_{iso} value of the parent atom. Structure validation, ORTEP illustration and drawing of packing diagrams were performed with PLATON.[17] Full details on data collection and structure refinement are provided in the Supporting Information (Crystallographic Tables). A summary of the data collection and refinement details is given in Table 1. CIF files containing the supplementary crystallographic data were deposited at the Cambridge Crystallographic Data Centre, with references CCDC 2110242 (polymorph 1) and 2110241 (polymorph 2).

Table 1 – Summary of the single-crystal X-ray data collections and crystal structure refinements.

	Polymorph **1**	Polymorph **2**
Chemical formula	$C_{13}H_9N_3O_3$ S	=
Formula weight	287.29	=
Color	Burgundy	Orange
Space group	$P2_1/n$	$P2_1/c$
Cell volume (Å^3)	1295.51(8)	2610.4(4)
Crystal system	monoclinic	monoclinic
a (Å)	5.3354(2)	25.451(3)
b (Å)	14.2344(4)	14.4966(14)
c (Å)	17.1709(6)	7.1113(7)
α (deg)	90	90
β (deg)	96.567(2)	95.795(6)
γ (deg)	90	90
Z/Z'	4/1	8/2
D_c (Mg m^{-3})	1.473	1.462
Radiation (Å) (graphite monochromated)	0.71073	0.71073
Max. crystal dimensions (mm)	0.32×0.25×0.22	0.50×0.13×0.12
Θ range (deg)	3.729 – 27.498	2.413 – 24.999
Range of *h*, *k*, *l*	–6,6;–18,18;–22,22	–30,30;–17,17;–8,8
Reflections measured/independent	122630/2963	207226/4598
Reflections observed ($I > 2\sigma$)	2292	4598/3090
Data/restraints/parameters	2963/0/185	4598/0/369
GOF	1.062	1.099
R_1 ($I > 2\sigma$)	0.0417	0.0584
wR_2	0.11181	0.1582
Function minimized	$\Sigma\, w\,(\|F_o\|^2 - S\|F_c\|^2)$	$\Sigma\, w\,(\|F_o\|^2 - S\|F_c\|^2)$
Diff. density final max/min (*e* Å^{-3})	0.273, –0.192	0.374, –0.260

X-ray powder diffraction data was collected on a Bruker D8 Advance diffractometer equipped with a LYNXEYE linear position sensitive detector and using Ni-filtered Cu Kα radiation (λ = 1.54059 Å).

The data was measured in Bragg-Brentano geometry covering the 2θ range 5-60°, using an angular step of 0.01° and counting 5 s/step. Indexation of the powder diffraction pattern of polymorph 3 of AcROYwas done using the LP-search algorithm[18] as implemented in the TOPAS V software,[19] consisting of a set of Monte-Carlo searches for the lattice parameters, followed by a Pawley refinement at the end of each Monte-Carlo search. This algorithm uses a suitable figure of merit to find local minima robust to small deviations from the correct lattice parameters, which is also used as a penalty in the initial cycles of the non-linear least-squares Pawley refinement to ensure proper convergence.

The differential scanning calorimetry (DSC) experiments were performed using a Perkin Elmer Pyris-1 power compensation calorimeter, equipped with a 1:1 v/v ethylene glycol:water cooler at −25 °C and a 20 mL min^{-1} nitrogen purge flow. Hermetically-sealed aluminum pans were used (samples weighting between 1 and 2 mg), with an empty pan used as reference. The temperature and enthalpy calibrations were performed with indium (Perkin Elmer, 99.99%, T_{fus} = 156.6 °C; $\Delta_{fus}H_m$ = 3286 ± 13 J·mol^{-1}) and caffeine (Mettler Toledo calibration substance, ME 18872, T_{fus} = 235.6 ± 0.2 °C). The samples were scanned from 25 to 210 °C at a scan rate of 10 °C min^{-1}.

Polarized light thermal microscopy (PLTM) experiments were performed using a Linkam DSC600 hot stage, with a Leica DMRB microscope and a Sony CCD-IRIS/RGB video camera. Images at 50× magnification were collected in heating runs carried out at a scan rate of 10 °C min^{-1} and analyzed with LinkSys software by Linkam.

Density Functionl Theory (DFT) calculations and Hirshfeld analysis

The DFT calculations were performed using the Gaussian 09 program (version D.01)[20] on the isolated molecule of the compound, and included the geometry optimization of each low-energy intramolecularly H-bonded conformer, energy scans associated with the conformationally relevant torsional coordinates, and calculation of the vibrational spectra (IR and Raman) of the AcROY molecule. The three-parameter B3LYP density functional, with the Becke's gradient exchange correction[21] and the Lee, Yang and Parr correlation functional was used,[22] together with the 6-311++G(2d,p) basis set.[23]

The Hirshfeld analysis was performed with CrystalExplorer 17.5,[24] using as input the CIF files of the two polymorphs whose crystal structure could be solved. The mapping that summarizes the Hirshfeld analysis results were built from the normalized contact distances, d_{norm}, which is calculated from the distances of a given point of the Hirshfeld surface to the nearest atom outside, d_e, and inside, d_i, the surface, as defined by Equation 1, where r^{vdW} represent the van der Waals radii:[25–29]

$$d_{norm} = \frac{d_i - r_i^{vdW}}{r_i^{vdW}} + \frac{d_e - r_e^{vdW}}{r_e^{vdW}} \quad (1)$$

Results and Discussion

Conformational analysis of the isolated AcROY molecule

As mentioned in the introduction section, AcROY molecule has essentially two internal degrees of freedom that are conformationally relevant, θ and φ, which correspond to the rotations around the N–C(thiophene) and C(thiophene)–C(acetyl) bonds, respectively (see Scheme 1). As for other structurally related molecules including ROY,[1-10] the nitrophenyl fragment in the low-energy conformers of AcROY is kept nearly co-planar with the NH bridging bond as a result of the presence in these forms of a stabilizing intramolecular N–H···O hydrogen bond, which blocks the conformational flexibility around the C–N bond connecting these two fragments. In turn, the acetyl substituent can assume 3 equivalent geometries, corresponding to a 3-fold rotor, but this rotation does not contribute to increase the number of distinct conformers of the molecule (though it multiplies the number of minima on the potential energy of the molecule by 3). The conformational search was then performed scanning along both the θ and φ coordinates.

Four different low-energy intramolecularly H-bonded conformers were identified, which are presented in Figure 1. All conformers are C_1 symmetry and have a symmetry equivalent form (as mentioned, each structure correspond to 3 degenerate minima resulting from the 3 possible orientations of the methyl group, so that the total number of minima on the potential energy surface of AcROY associated with the 4 conformers is 24). The four conformers are here designated as **A**, **B**, **C** and **D**, following an increasing order of energy.

The two most stable conformers (**A** and **B**) present the oxygen atom of the acetyl substituent turned to the same side of the sulfur atom of the thiophene ring (φ, as defined by the C3–C4–C5=O1 dihedral angle, being equal to 178.6 and 178.9º, respectively; see Figure 1 for atom numbering, and Table 2), and differ from each other regarding the conformation defined by the θ coordinate: in the most stable conformer **A**, the sulfur atom of the thiophene ring is turned to the opposite side of the N–H bridging bond (θ = 169.5º, as defined by the C8–N2–C1=C2 dihedral angle), while in conformer **B** it is turned the opposite direction (θ = 46.0º). Conformer **A** is 6 kJ mol^{-1} lower in energy than **B**, mostly because of the presence in conformer **B** of the unfavorable steric interaction between the cyano substituent of the thiophene ring and the closely located hydrogen atom (H9) of the nitrophenyl ring. Conformers **C** and **D** are the counterparts of forms **A** and **B**, respectively, having the acetyl group turned to the opposite side of the sulfur atom of the thiophene ring. In these conformers, θ and φ are equal to 170.0 and 1.7º (**C**) and 49.8 and 4.1º (**D**). Conformer **C** is more stable than **D** by 2.5 kJ mol^{-1}. Compared to the most stable conformer **A**, the relative energies of conformers **C** and **D** are 9.8 and 12.3 kJ mol^{-1}, respectively. The lower energy of the two conformers, **A** and **B**, compared to **C** and **D**, results mostly from the existence in the first two forms of a stabilizing O···S

interaction (see Figure 1), following the trend observed previously for other molecules where this type of interaction was found to be relevant in structural terms.[30-32]

It is interesting to point out that in all the four conformers, the intramolecular hydrogen bond connecting the N–H bridging group to the nitro substituent of the phenyl ring shares identical structural features, the O···HN hydrogen bond distance and the O···H–N angle varying in the short ranges of being 1.798-1.805 Å and 132.9-133.7º.

Table 2 – Values of the C8–N2–C1=C2 (θ) and C3–C4–C5=O1 (φ) dihedral angles and relative energies (ΔE) of the four low-energy conformers of AcROY.

Conformer	C8–N2–C1=C2 (θ)/ º	C3–C4–C5=O1(φ)/º	ΔE/ kJ mol^{-1}
A	169.5	178.6	0.0
B	46.0	178.9	6.0
C	170.0	1.7	9.8
D	49.8	4.1	12.3

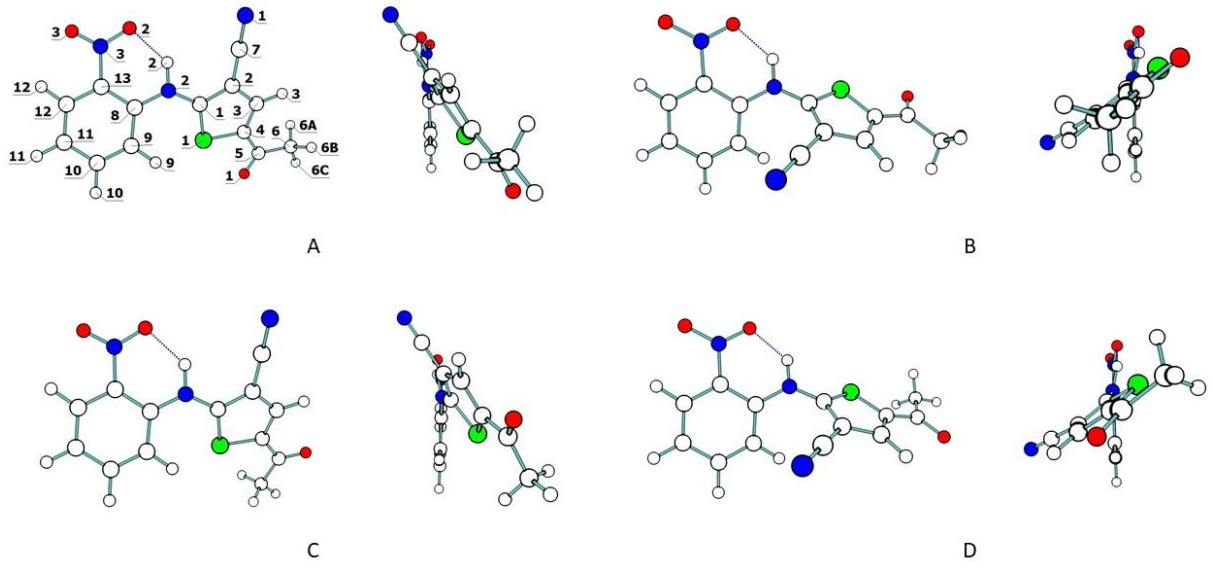

Figure 1 – Geometries of the four low-energy intramolecularly H-bonded conformers of AcROY with the adopted atom numbering (two images are presented for each conformer, corresponding to views from two different perspectives). Each of the represented structures has a symmetry-equivalent form (considering also the 3 degenerated minima resulting of the internal rotation of the methyl group for each symmetry-equivalent structure, the number of minima associated to each one of the conformers represented in the figure is in fact 6, on a total of 24 minima). For relative energies and values of the conformationally relevant dihedral angles, see Table 2.

Figures 2 and 3 show the calculated potential energy profiles for the interconversion between the AcROY conformers. Figure S4 (Supporting Information) presents in a compact form the relevant data regarding relative energies and interconversion barriers for the low energy conformers of AcROY.

In Figure 2, the scan coordinate is θ, which is associated with the interconversions between two different pairs of conformers: **A** and **B** (with the acetyl substituent in one orientation), and **C** and **D** (with the alternative orientation of the acetyl group). The two obtained energy curves show similar profiles. When considering the interconversion between **A** and **B** forms, we started the scan at the geometry of **A'** (*i.e.*, the equivalent-by-symmetry structure of that representing conformer **A** in Figure 1) and varied the scan coordinate in increments of 10º, while optimizing all the remaining structural parameters. Form **A'** first converts into **B'**, through an energy barrier of only 11.1 kJ mol^{-1}. Subsequently, the energy increases progressively while the molecule tends to co-planarity of the two rings (nitrophenyl and substituted-thiophene). However, the putative co-planar structure is highly strained due to the close contact it implies between the cyano substituent of the thiophene ring and the phenyl moiety, so that at a certain point (when θ is ~30º) inversion at the bridging nitrogen atom takes place. This inversion at the N atom of the bridge leads to an abrupt decrease in energy, and takes the molecule to the potential energy well of conformer **B**. The maximum energy reached along the scan from **B'** to **B** was *ca.* 28 kJ mol^{-1}. From **B**, the molecule can then be converted into **A** through a barrier of 5.1 kJ mol^{-1}, the transition state for this transformation being equivalent-by-symmetry to that of the conversion of **A'** into **B'**. Finally, interconversion between the two symmetry-related **A** and **A'** structures takes place through a small barrier of only 0.7 kJ mol^{-1}. In practical terms, the global format of the potential energy profile allows to conclude that interconversion between the 4 structures **A**, **B**, **B'**, **A'** can take place easily through barriers that are not larger than 11.1 kJ mol^{-1}, demonstrating the flatness of the torsional potential of AcROY along θ. The same conclusions can be extracted by taking into account the potential energy profile interconnecting forms **C**, **D**, **D'** and **C'** (see Figure 2). In this case, the barrier for **C**→**D** conversion is 6.6 kJ mol^{-1} (4.1 kJ mol^{-1} in the reverse direction) are and that between the two equivalent **C** forms is 0.8 kJ mol^{-1}, while the maximum energy value for the **D'**→**D** conversion obtained along the performed scan was ~25 kJ mol^{-1}.

Figure 3 shows the potential energy profiles for rotation of the acetyl substituent obtained when the conformation around the N–C(thiophene) bond was kept at values characteristic of the conformers of AcROY. The two curves represent the interconversion paths between conformers **A** and **C** and conformers **B** and **D**. Because the geometry around the N–C(thiophene) bond is skewed, for both A-C and B-D conversions, the internal rotation of the acetyl group can take place by two different pathways, which correspond to rotation of the acetyl group in the two possible directions. As it can be seen in Figure 3, however, all the four pathways (the two interconverting **A** and **C** and the two interconverting **B** and **D**) are very similar, with the barriers separating **A** and **C** being slightly higher than those separating **B** and **D** (43.6 and 42.3 kJ mol^{-1}, *vs.* 38.2 and 36.7 kJ mol^{-1}, respectively, taken from the corresponding lower energy conformer). It is worth noticing that these barriers are larger than those associated with the rotation around the N–C(thiophene) bond (see Figures 2,3 and S4).

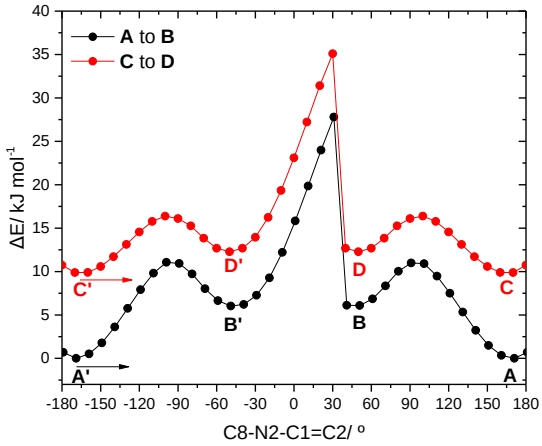

Figure 2 – Potential energy profiles associated with the internal rotation θ, as defined by the dihedral angle C8–N2–C1=C2, in keeping the conformation of the acetyl group in two different orientations. The arrows indicate the direction of the performed scans; **A'**, **B'**, **C'** and **D'** are the symmetry-equivalent structures of **A**, **B**, **C** and **D**, respectively (see text for details).

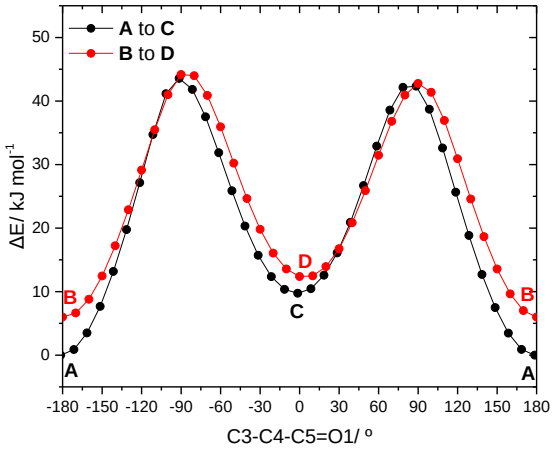

Figure 3 – Potential energy profiles associated with the internal rotation φ, as defined by the dihedral angle C3–C4–C5=O1, in keeping the conformation around the N–C(thiophene) in two different orientations (see text for details).

Polymorphs screening

After the synthesis of the compound, accomplished as described in the Materials and Methods section, the search for different polymorphs was undertaken. Two different approaches were used: the first one consisted in the recrystallization of the compound from solvents of different polarity, by slow evaporation of the solvent at room temperature; the second was by slow cooling of the melted compound. However, the latter resulted in the production of an amorphous phase, possibly due to partial degradation of the sample, which inhibited further investigation.

The solvents used are listed in Table S1 (Supporting Information), together with the corresponding obtained AcROY crystalline materials. Solids of three different morphologies and colors were obtained,

which points out to three different polymorphs that are depicted in Figure 4. The burgundy elongated-plate shape crystals labeled as **1** in Figure 4 were obtained from all used solvents. On the other hand, the orange needle shape crystals **2** were only obtained from recrystallization from acetone, always in concomitant mixtures, and the agglomerates formed by the small-sized orange-yellowish needles **3** were obtained from both acetone and DMSO, also in concomitant mixtures.

Figure 4 – The three different AcROY crystalline materials obtained in the polymorph screening experiments. Images are 10× amplified.

Infrared and Raman spectroscopy characterization of the AcROY polymorphs

The three different polymorphs of AcROY were morphology-based selected and characterized by both infrared (in ATR mode) and Raman spectroscopies. Figures 5 and 6 show the room temperature Raman and IR spectra of the three polymorphs, which show clearly distinctive vibrational signatures, in spite of the general resemblance of the spectra. Table S2 lists the major observed bands together with their tentative assignments made with help of the results of theoretical calculations of the spectra performed for the isolated molecule of the compound (conformer **A**, the conformer that is present in the crystals, according to the performed X-ray diffraction studies described in the next section).

The molecule of AcROY is C_1 symmetry, and the correlation method applied to the vibrations of the crystals of polymorphs **1** and **2**, whose structure could be obtained by single crystal X-ray diffraction crystallography (see next section), renders the representations $81A_g+81B_g+81A_u+81B_u$ (polymorph **1**) and $162A_g+162B_g+162A_u+162B_u$ (polymorph **2**) for the symmetry of the intramolecular vibrations. Besides, 24 and 48 modes, respectively for **1** and **2**, are intermolecular in nature, with the 3 acoustic modes being A_u+2B_u symmetry for both crystals and the intermolecular optical modes $6A_g+6B_g+5A_u+4B_u$ and $12A_g+12B_g+11A_u+10B_u$, respectively. This means that under the crystal symmetry, the rule of mutual exclusion applies to the vibrational spectra of both polymorphs **1** and **2**, and the modes active in IR (A_u and B_u) are silent in Raman, while those active in Raman (A_g, B_g) are not observable in infrared, so that a total of 162 modes are expected to contribute to the IR and Raman spectra of polymorph **1** and 324 modes to the

spectra of polymorph **2**. Despite of the non-coincidence of vibrations in IR and Raman predicted by the symmetry analysis, one can expect the Davidov splitting to be small for most of the modes, and thus the bands of related vibrations active in IR or Raman shall be nearly coincident. The same can also be expected for most of the related modes active either in IR and Raman belonging to different symmetry species, *i.e.*, A_u and B_u modes associated with the same coordinates in the one side and A_g and B_g modes associated with the same coordinates in the other side. As a whole, the number of expected bands in the spectra of the two polymorphs shall not be much larger than the number of vibrations of the isolated molecule of the compound (81). Since the crystal structure of polymorph **3** could not be solved, the symmetry analysis of the vibrations of this polymorph could not also be undertaken. In any case, the number of quasi-degenerated modes can also be expected to be large for this crystal, by the same reasons mentioned above, so that as for polymorphs **1** and **2**, the number of observable bands in the vibrational spectra of polymorph **3** can also be predicted not to be much larger than that for the isolated molecule of the compound. In Table S2, the vibrational spectra of the AcROY polymorphs are interpreted based on these assumptions, and the calculated spectrum of the isolated molecule of the compound (conformer **A**) was used as reference. Though being a rough simplification, this approach seems to be reasonable in the present case, also because the intermolecular interactions in the crystals can be expected to be relatively weak (no strong hydrogen bonds are present) and, thus, should perturb only in a very small extent the intramolecular vibrational potential.

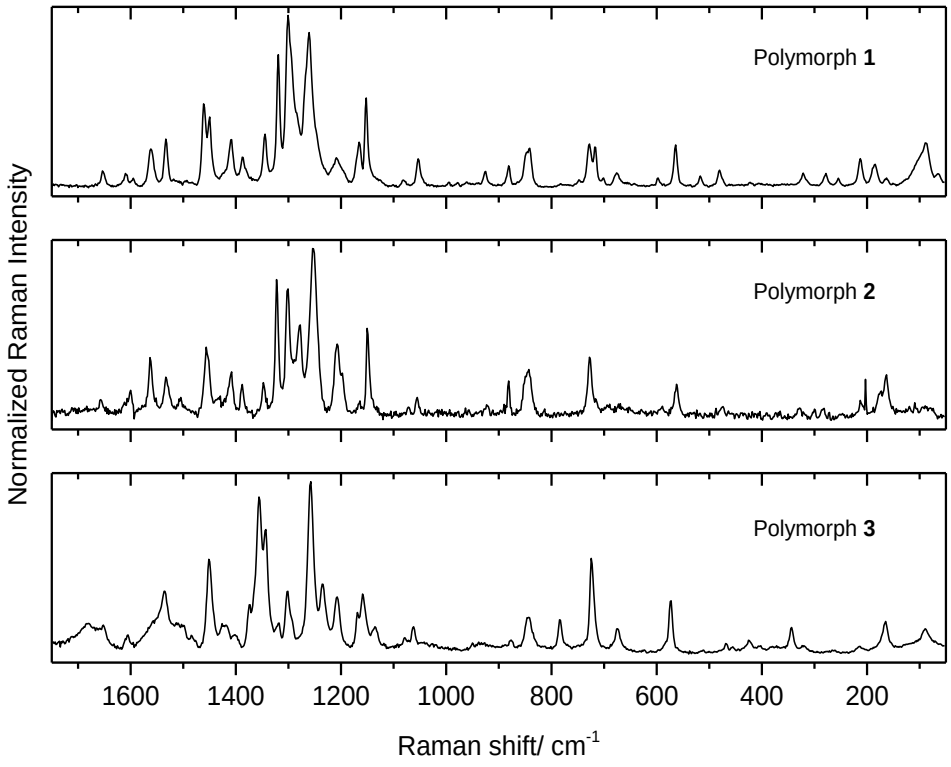

Figure 5 – Room temperature Raman spectra of the three observed AcROY polymorphs, in the 50-1750 cm^{-1} range.

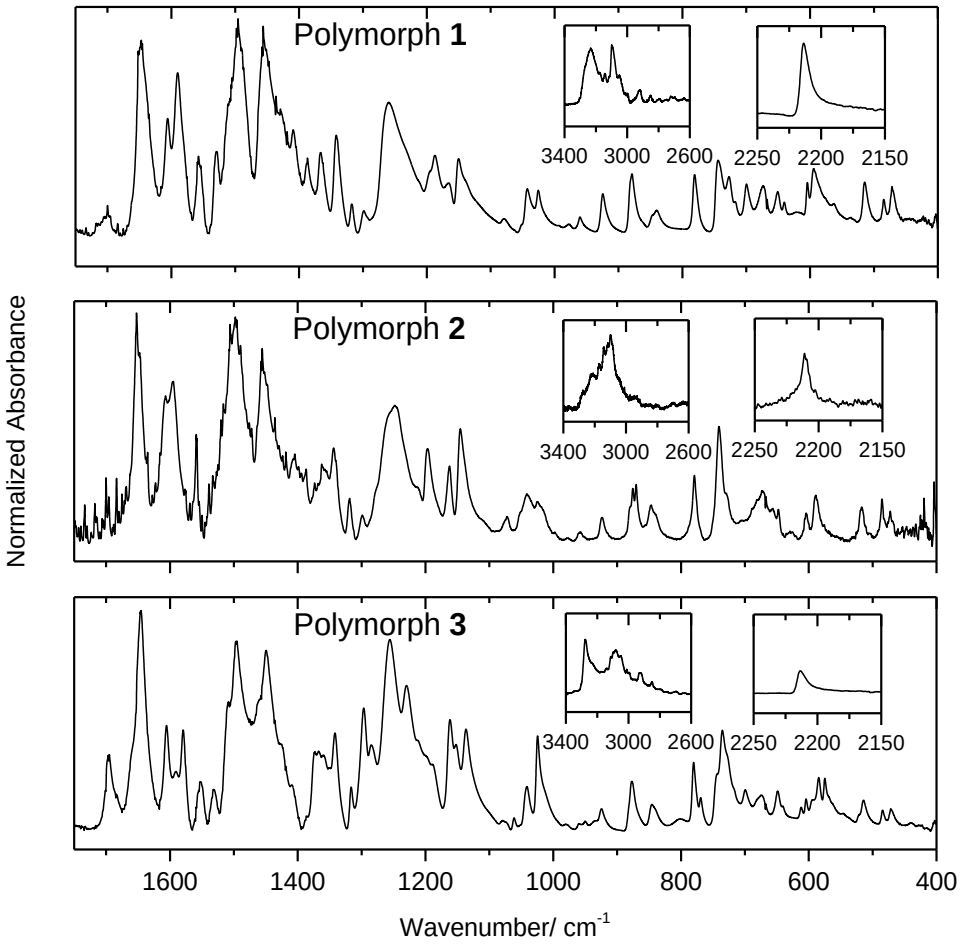

Figure 6 – FTIR spectra (ATR mode) of of the three observed AcROY polymorphs, in the 1750-400 cm^{-1} range; the 3400-2600 and 2250-2150 cm^{-1} regions are shown as in-sets.

In the context of the present work, the identification of band-marks of each of the polymorphs is of particular interest. The intense bands observed in the 1100-1400 cm^{-1} range in both the IR and Raman spectra of the polymorphs appear particularly suitable for this goal. In the case of the Raman spectra, the most intense bands in this spectral region appear at 1319, 1301 and 1261 cm^{-1}, for polymorph **1**, at 1322, 1302, 1278 and 1253 cm^{-1}, for polymorph **2**, and 1356, 1344 and 1258 cm^{-1} for polymorph **3**, and can be used for fast identification of the polymorphs by using this technique. In infrared, bands at 1260, 1188 and 1150 cm^{-1} (**1**), 1248, 1196, 1162 and 1146 cm^{-1} (**2**) and 1256, 1230, 1162 and 1137 cm^{-1} (**3**) appear as good identifiers of the polymorphs.

Though a detailed discussion of the vibrational spectra of the materials is not to be done here, it is interesting to note that the frequencies at which the ν(C≡N) stretching vibration is observed in the three polymorphs of AcROY are consistent with a small angle between the two rings of the molecules in the crystals, and also with their colors, according to the relationship between these properties recently presented

by Tang and co-workers.[33] Those authors have found that in the red and most of the orange polymorphs of ROY the ν(C≡N) stretching mode appears in the 2205-2220 cm^{-1} wavenumber range, while in the yellow polymorphs this mode gives rise to a band in the 2220-2235 cm^{-1} wavenumber range. In AcROY, this mode is observed at 2214 (in **1**), 2211 (**2**) and 2213 (**3**) cm^{-1} (see Table S2) as expected considering the burgundy, orange and orange-yellowish colors they exhibit. This is also in consonance with the small angles between the planes of the two rings observed in the crystals of polymorphs **1** and **2** [28.32(9)º in polymorph **1**, and 5.55(13)º and 13.63(14)º in the two different types of molecules found in the crystal of polymorph **2**, as detailed in the next section].

Crystallographic structures (polymorphs **1** and **2**)

Suitable crystals for single crystal X-ray diffraction structural studies were obtained for polymorphs **1** and **2**. Unfortunately, in the case of polymorph **3** the obtained crystals were not of good enough quality for this type of experiments. The X-ray data showed that both polymorphs **1** and **2** crystallize in the monoclinic, centrosymmetric space group Nº 14, the unit cell used in the data-collections corresponding to the space-group settings $P2_1/n$ for polymorph **1** and $P2_1/c$ for polymorph **2**. Polymorph **1** has one symmetry independent molecule in the unit cell ($Z = 4$; $Z' = 1$) whereas the unit cell of polymorph **2** has a volume twice as large as that of polymorph **1** and corresponds to a structure with two symmetry independent molecules in the unit cell ($Z = 8$; $Z' = 2$). A thorough check with the tools available in PLATON[17] did not reveal any missing symmetry in the larger unit cell. The two symmetry independent molecules in the unit cell of polymorph **2** are enantiomorph pairs that can closely match after inversion followed by a (non-crystallographic) pseudo glide-plan. ORTEP plots showing the anisotropic displacement ellipsoids and depicting the molecular conformation in the crystals of polymorphs **1** and **2** are presented in Figure S5.

For both polymorphs of AcROY studied using single crystal X-ray diffraction crystallography, the determined bond distances and valence angles in the molecules fall within the range of expected values of similar compounds (see Table S3 in Supporting Information). The N–O bond distances are in the range 1.208–1.225 Å, the longer values corresponding to those bonds involved in the intramolecular hydrogen-bonding with the N–H bridging group, as expected. The N–C bond distances of the amine bridge are significantly asymmetric [1.358(3)/1.385(3) Å], the shorter distance being towards the thiophene ring, in line with the calculated values for the isolated molecule of the compound (1.367 and 1.385 Å). The thiophene C–S–C angle is slightly larger than 90°, also in agreement with the calculated data for the isolated molecule (91.46º).

The two rings, that are strictly planar within experimental error, are not coplanar, the angle between their least-squares planes being larger for the molecule in polymorph **1** [28.32(13)°] than for the two distinct AcROY molecules in polymorph **2** [5.55(9)º and 13.63(14)º]. In fact, both molecules in polymorph **2** are

more planar than in polymorph **1**, with the angle between the planes of the phenyl group and of the nitro substituent being 17.0(3)º in polymorph **1** and only 2.7(2) and 1.1(4)º in polymorph **2**, those between the planes of the thiophene ring and the acetyl group being 176.0(2)º (**1**) and 177.9(4) and –179.4(5)º (**2**), and the C1–N2–C8–C9 dihedral angle being –24.6(4)º in **1** and –5.6(6) and –15.3(6)º in **2**. The strong intramolecular hydrogen bond established between the nitro group and the amine bridge is preserved in the crystals, restricting the conformational flexibility of the nitro substituent and around the N2–C8(phenyl) bond, but, like for the isolated molecule, significant deviations from planarity of the O_2N-Phe-NH fragment are observed in both polymorphs mostly due mostly to steric hindrance between the two rings (Table 3). It is interesting to note that, compared to the isolated molecule of AcROY (conformer **A**), where according to the performed DFT calculations the C1–N2–C8–C9 dihedral angle is –19.5º, this dihedral angle increases in polymorph **1** and decreases in polymorph **2** due to intermolecular packing. The same trend is observed for the deviation of the nitro group from the ring plane (as measured by the C8−C13−N3−O2 dihedral), which increases in polymorph **1** and reduces in polymorph **2** compared to the isolated molecule, where the C8−C13−N3−O2 dihedral predicted by the DFT calculations is 11.4º (in conformer **A**). Note that recent studies in ROY[34,35] have concluded that DFT approaches provide reliable molecular geometries for this type of compounds (though not so precise conformational energy differences, tending to over-stabilize the more planar structures). As for ROY,[34,35] the present study indicates that both the small deviations from the nitro group from the plane of the ring and the non-coplanarity of the fragments around the N2–C8 bond are not solely due to intermolecular packing, though they are modulated in some extent by intermolecular interactions in the crystals.

Table 3 – Values of the relevant dihedral and torsion angles of polymorphs **1** and **2**. The first column of polymorph **2** corresponds to the molecule with unprimed atomic labels, and the second column to the molecule with primed labels (see Figure 8).

Dihedral/torsion angle/ °	Polymorph **1**	Polymorph **2**	
< (S1C1...C4)/(C8C9…C13)	28.32(9)	5.55(13)	13.63(14)
< (C8C9...C13)/$N3O_2$	17.0(3)	2.7(2)	1.1(4)
< (S1C1...C4)/(C4C5C6O1)	5.11(16)	1.74(18)	4.04(12)
C8−N2−C1=C2 (θ)	177.7(2)	−171.1(4)	−175.5(4)
C3−C4−C5−O1 (φ)	176.0(2)	177.9(4)	−179.4(5)
C1−N2−C8−C9	−24.6(4)	−5.6(6)	−15.3(6)
C8−C13−N3−O2	18.6(3)	2.2(6)	−0.4(6)

Inspection of close contact distances and angles shows the presence of an extensive 3D network of intermolecular hydrogen bonds in both polymorphs, which are depicted in Figure 7 (polymorph **1**) and Figure 8 (polymorph **2**). The only strong donor group in the molecule is the amine group that is involved in the above-mentioned intramolecular interaction with the nitro group. All the other intermolecular short

contacts can be classified as weak non-classic hydrogen bonds of the C_{aryl}–H···O, C_{aryl}–H···N, C_{aryl}–H···S or C_{methyl}–H···O types. These interactions are detailed in Tables 4 and 5 for polymorphs **1** and **2**, respectively. In polymorph **1**, every possible acceptor atom is involved in one such interaction, while in polymorph **2** only atom O3 is not involved in the hydrogen bond network. In both polymorphs, the molecules pack in layers, the hydrogen bonds being established mainly within the layers. Cohesion between the layers is achieved by van der Waals interactions and interactions between the π-electron clouds of nearly stacked rings. In the case of polymorph **2**, in addition to these ring interactions, one C–H···O hydrogen bond also interconnects the layers as shown in Figure 8b. A remarkable difference between the molecular packing in the two polymorphs is the occurrence of a somewhat short S···S contact [3.585 Å] in polymorph **2**, that can be observed in Figure 8b, and that is absent in the structure of polymorph **1**. Noteworthy, the S···S contact found in the polymorph **2** of AcROY is considerably shorter than all S···S distances found in the different polymorphs of the parent compound ROY whose structure has been solved, which vary within 3.945 Å (in the so called ON – orange needle –polymorph) and 5.582 Å (in the Y – yellow – polymorph).[2,5,14,36]

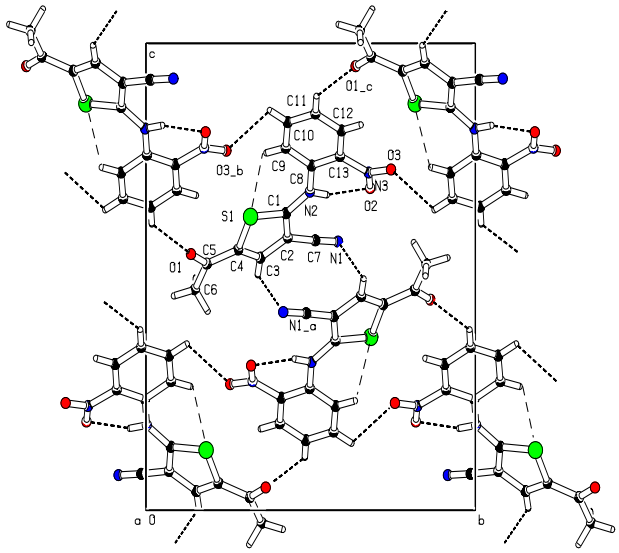

Figure 7 – Hydrogen-bonding network in polymorph **1**. The view is a projection along the crystallographic *a*-axis. Intramolecular C−H···S short contacts are shown as long dashes.

Table 4 – Hydrogen bonds and short intermolecular contacts in polymorph **1**. Distances and angles are given in Å and degrees, respectively; D and A represent the hydrogen bond donor and acceptor atoms, respectively.

D−H···A	D−H	H−A	D···A	< D−H···A
N2−H2···O2	0.82(3)	1.94(3)	2.612(2)	139(3)
C9−H9···S1	0.93	2.50	3.319(3)	147
C3−H3···N1[a]	0.93	2.53	3.132(2)	123
C10−H10···O3[b]	0.93	2.52	3.061(3)	117
C11−H11···O1[c]	0.93	2.45	3.213(3)	139

Symmetry codes: a) −1−*x*,1−*y*,1−*z*; b) 3/2−*x*,-1/2+y,3/2−*z*; c) 3/2−*x*,1/2+*y*,3/2−*z*.

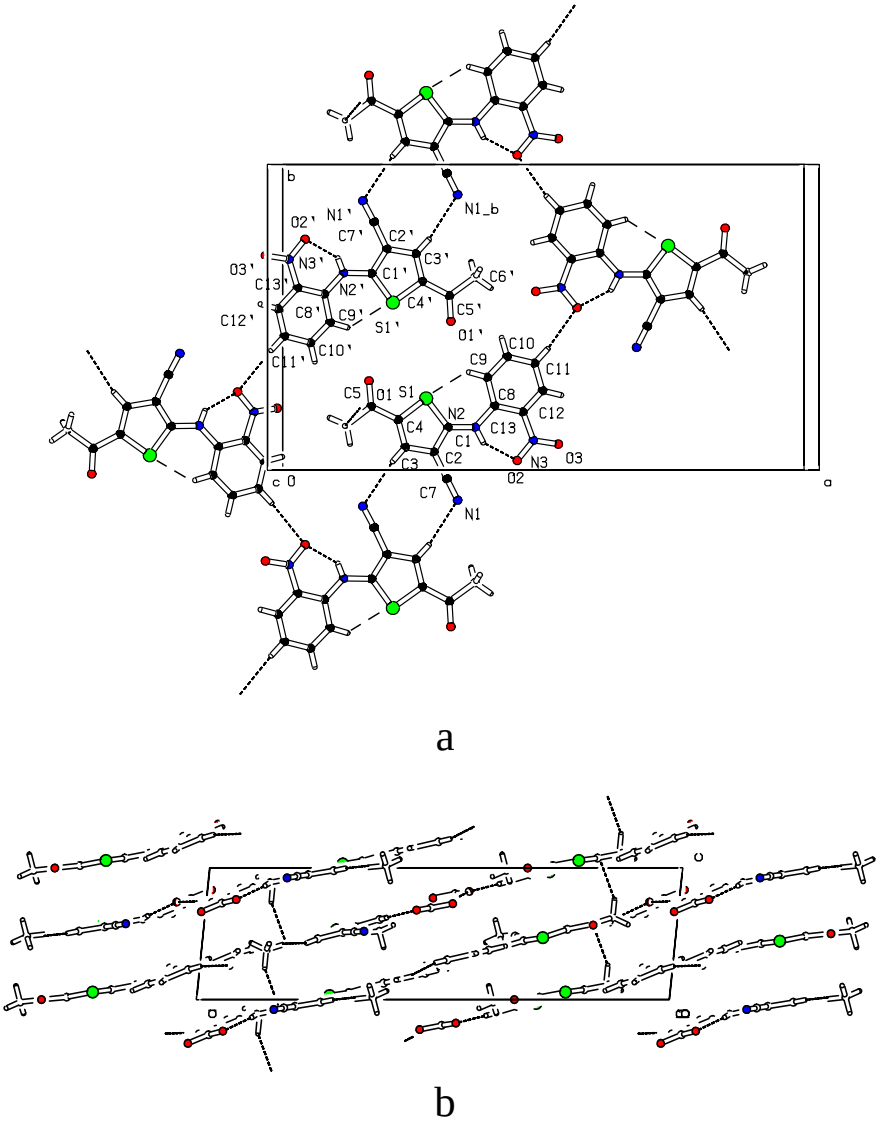

Figure 8 – Hydrogen-bonding network in polymorph **2**. (a) Projection along the crystallographic *c*-axis; (b) projection along the crystallographic *b*-axis. Intramolecular C−H…S short contacts are shown as long dashes.

Table 5 – Hydrogen bonds and short intermolecular contacts in polymorph 2. Distances and angles are given in Å and degrees, respectively.

D−H···A	D−H	H−A	D···A	< D−H···A
N2−H2···O2	0.83(4)	1.87(4)	2.588(4)	145(4)
N2'−H2'···O2'	0.78(4)	1.94(4)	2.591(4)	142(4)
C9−H9···S1	0.93	2.43	3.147(4)	134
C9'−H9'···S1'	0.93	2.46	3.153(4)	132
C3−H3···N1'[a]	0.93	2.55	3.461(5)	165
C3'−H3'···N1[b]	0.93	2.53	3.448(6)	169
C11−H11···O2[c]	0.93	2.51	3.426(5)	170
C11'−H11'···O2'[d]	0.93	2.55	3.467(5)	170
C6−H6B···O1[e]	0.96	2.48	3.323(6)	146

Symmetry codes: a): *x*, −1+*y*,*z*; b) *x*,1+*y*,*z*; c) 1−*x*,1/2+*y*,1/2−*z*; d) −*x*,-1/2+*y*,3/2−*z*; e) *x*,1/2−*y*,1/2+*z*.

For polymorph **3** it was not possible to obtain suitable crystals for single crystal X-ray diffraction structure determination. Nevertheless, powder X-ray measurements were undertaken for this polymorph. The powder diffraction pattern obtained for polymorph **3** is compared with the simulated powder patterns of polymorphs **1** and **2** derived using the corresponding X-ray structural data in Figure 9. Indexing of the powder pattern of polymorph **3** resulted in a solution with lattice parameters a = 11.383(3) Å, b = 13.6609(3) Å, c = 25.247(7) Å, β =101.75(1) (monoclinic) that could successfully index all peaks in the diffractogram (see Figure S6 in the Supporting Information). The molar volume of polymorphs **1** and **2** is approximately 325 Å^3 per molecule, while the volume of the unit cell found for polymorph **3** is 3843 Å^3, giving a total of 12 molecules per unit cell, assuming the same molar volume. As the most likely space group of polymorph **3** is nº 14 ($P2_1/c$), with Z = 4, this would correspond to a structure with Z' = 12/4 =3. No satisfactory solution was found with unit cells of lower volume during many Monte-Carlo runs, and other indexing methods failed due to the strong overlap of diffraction peaks. Even if one cannot exclude that the unit cell found is a supercell of the true cell of polymorph **3**, as the local minimum found by the Monte-Carlo may not be the global minimum, the larger unit cell found points to a more complex supramolecular structure of polymorph **3** compared to those of polymorph **1** and **2**.

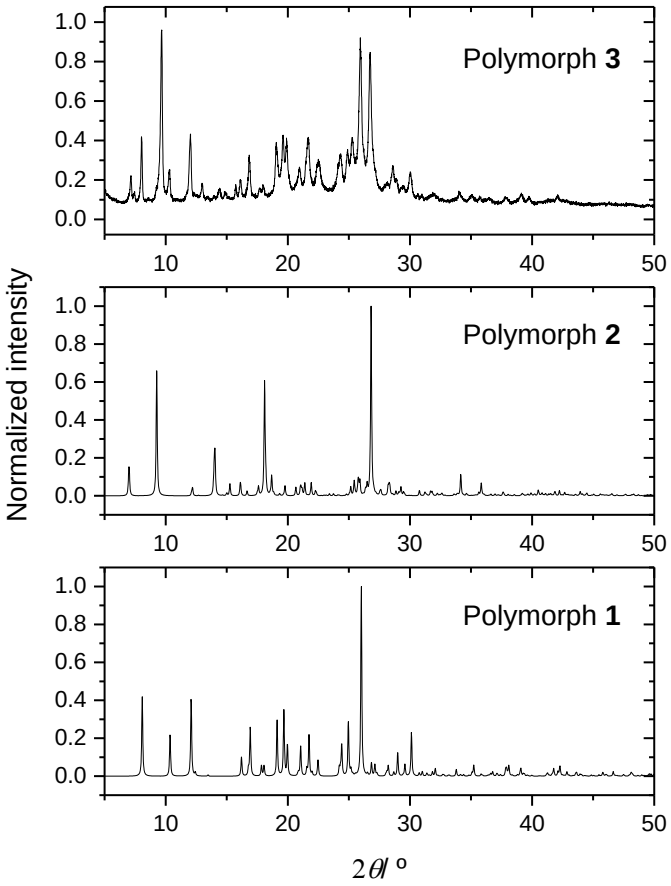

Figure 9 – Powder X-ray diffractograms for the polymorphs of AcROY. Data for polymorphs **1** and **2** were simulated using the solved crystal structure of the polymorphs; data for polymorph **3** were obtained experimentally.

Hirshfeld surfaces analysis

The study of crystallographic structures based on Hirshfeld surfaces, developed by Spackman and co-workers is an elegant effective approach to understand intermolecular interactions in a crystal and to evaluate crystal packing.[37] Hence, to characterize the intermolecular environments in polymorphs **1** and **2**, the Hirshfeld surface analysis of these structures was performed. Figure 10 presents the calculated Hirshfeld surfaces for the two polymorphs, with the intermolecular contacts given by the d_{norm} values, which range from –0.20 to 1.29 for polymorph **1** and from –0.19 to 1.34 for polymorph **2**. For polymorph **2**, the dimeric unit represented by the two molecules in the asymmetric unit of the crystal is considered in this analysis. Within the dimer, the most important interactions are the two pairs of non-classical hydrogen bond interactions C9–H9···O1 and C10–H10···O1. The red areas shown in the plots presented in Figure 10 represent the most important intermolecular interactions (shorter contacts) for each structure, which correspond to O3···H10–C10, O1···H11–C11, O1···$H6_A$–C6 and N1···H3–C3 intermolecular interactions in the case of polymorph **1**, and O3···$H6_A$–C6, O2···H11–C11, O3···$H6_C$–C6, O1···$H6_B$–C6 and N1···H3–C3 interactions in the case of polymorph **2**.

Table 6 presents the relative fractional areas (in %) of the Hirshfeld surfaces that are assigned to the different types of intermolecular interactions. The corresponding d_e vs d_i 2D-fingerpint plots are presented in the Supporting Information (Figures S6 and S7), together with the corresponding d_{norm} mapping on the Hirshfeld surfaces.

Taking into account the areas of the Hirshfeld surfaces assigned to the H···O/O···H contacts (29.1% for polymorph **1** and 22.1% for polymorph **2**), it is clear that the contribution of the non-classical intermolecular hydrogen bonds of the CH···O type to the stabilization of the crystal structure of polymorph **1** is more important than for polymorph **2**. On the other hand, the contribution of hydrogen bonds of the CH···N type to the stabilization of the crystal structure of polymorph **2** is considerably more significant than in polymorph **1** (H···N/N···H contacts fractional areas are 7.1% and 14.5% in polymorphs **1** and **2**, respectively). Interestingly, in consonance with the structural information directly extracted from the XRD data, the Hirshfeld surface analysis reveals also that, while in polymorph **1** there is no contribution of S···S intermolecular interactions to the stabilization of the crystalline lattice, in polymorph **2** there is a small, but still significant in structural terms, contribution of disulfide intermolecular contacts to the stabilization of the three-dimensional crystalline structure.

The data shown in Table 6 also show that dispersive interactions (as described in terms of short H···H and H···C/C···H contacts) are most probably also significant in stabilizing the two crystals, considering that the the H···C/C···H contacts account on total for 32.2% and 32.3% of the Hirshfeld surface areas of polymorph **1** and **2**, respectively. In polymorph **1**, the first type of interaction occurs essentially between the hydrogen atoms of the methyl group and the four phenyl hydrogen atoms of neighboring molecules,

while the H···C/C···H interactions refer to phenyl/phenyl stacking-type contacts between the partially superimposed rings of molecules in adjacent layers. Noteworthy, the C···C interactions occur essentially between the carbon atoms of the thiophene ring that do not bear any hydrogen atom (C1, C2) and that of the cyano group (C7) of each molecule and the same atoms of the neighboring molecules of adjacent layers, where the interacting moieties are oriented in an anti-parallel fashion relatively to the reference molecule. In polymorph **2**, H···H contacts involve mostly the methyl hydrogens and the phenyl hydrogen atom H11, which are not involved in interactions with oxygens, while the H···C/C···H interactions are associated with the same type of stacking contacts found in polymorph **1**. On the other hand, in polymorph **2** the C···C interactions are associated with the phenyl moiety of one of the molecules in the asymmetric unit, and predominantly with the carbon atom of the cyano group in the case of the second molecule. The different patterns found for the H···H and C···C interactions in the two polymorphs, clearly reveal the different arrangement of the molecules, in particular the neighborhoods of the phenyl and cyano substituent (for example, in the latter case, the anti-parallel orientation of the group in adjacent layers of molecules in the crystal of polymorph **1** is not preserved in polymorph **2**, where, otherwise, they are nearly perpendicular).

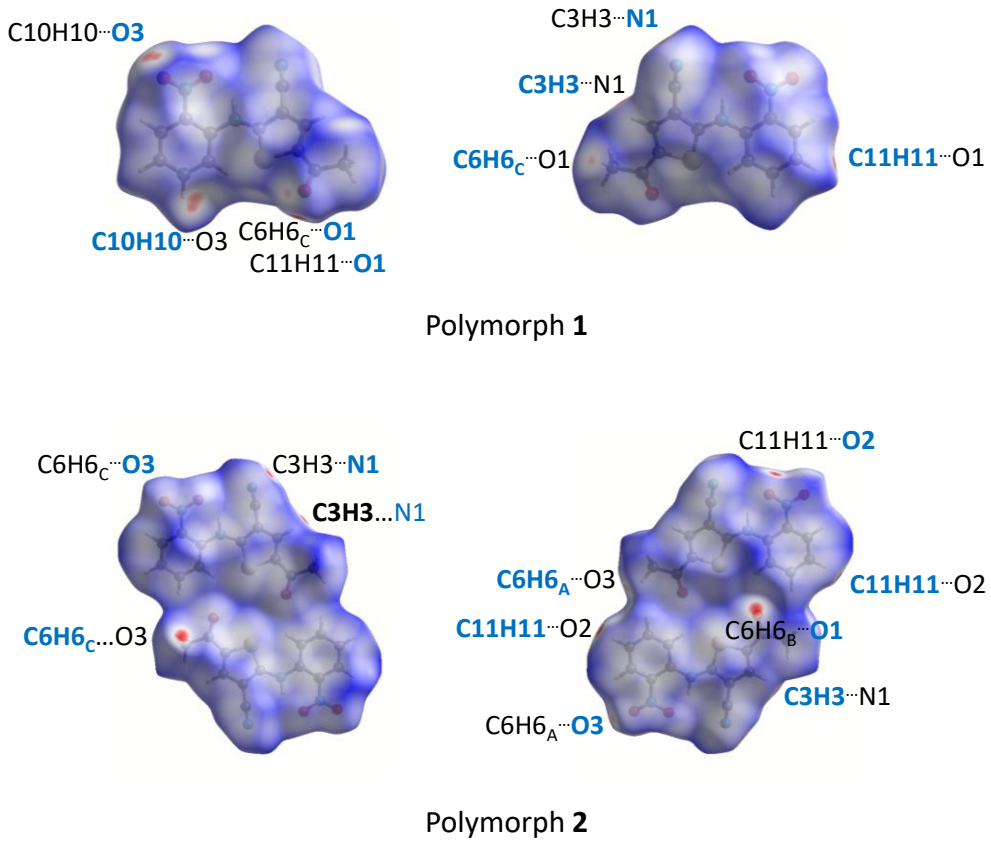

Figure 10 – d_{norm} mapping on the Hirshfeld surfaces of the molecules in polymorphs **1** and **2** of AcROY. Two different viewpoints are shown for each molecule, in the left column with the nitrobenzene group on the left-hand side (top molecule in the case of the Z'= 2 polymorph **2**), and in the right column with the nitrobenzene group on the right-hand side. Atoms participating in the indicated interactions that belong to neighboring molecules are notated in black.

Table 6 – Fractional areas (in %) of the Hirshfeld surface assigned to the different intermolecular interactions in AcROY polymorphs **1** and **2**.

Intermolecular interaction	Polymorph **1**	Polymorph **2**
H···O/O···H	29.1	22.1
H···H	20.9	18.6
H···C/C···H	11.3	13.7
C···N/N···C	7.2	4.8
H···N/N···H	7.1	14.5
C···C	7.1	8.2
H···S/S···H	4.4	2.3
C···O/O···C	3.7	4.9
N···N	2.4	0.9
C···S/S···C	1.8	3.5
N···O/O···N	1.4	2.8
O···S/S···O	1.4	0.4
N···S/S···N	1.3	0.5
O···O	1.0	2.2
S···S	0.0	0.7

Thermal analysis of the polymorphs

In order to study the thermal behavior of the identified polymorphs, crystal forms **1** and **3** were firstly investigated by differential scanning calorimetry (DSC). The melting of these polymorphs was observed at 200.3 ± 0.4 ºC (polymorph **1**) and 189.9 ± 1.4 ºC (polymorph **3**), as shown in Figure 11). The measured enthalpy of fusion was 32.7 ± 2.2 kJ mol^{-1}, for polymorph **1**, and 16.3 ± 2.0 kJ mol^{-1}, for polymorph **3**, which, according to the heat of fusion rule,[38-40] reveals that these two polymorphs are monotropically related, with polymorph **1** being the stable form and polymorph **3** the metastable crystal structure.

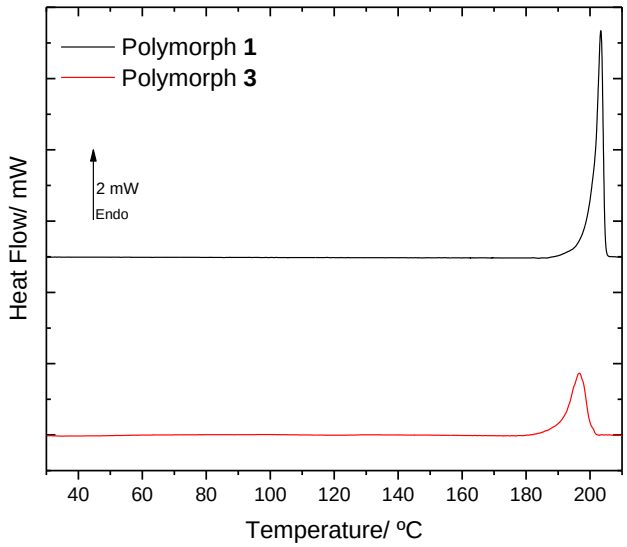

Figure 11 – DSC heating curves of polymorphs **1** and **3** of AcROY (heating rate: 10 ºC min^{-1}; masses: 1.10 mg, polymorph **1**; 1.11 mg, polymorph **3**.

Due to the lack of sufficient quantity of polymorph **2** to perform a DSC analysis, this crystallographic form was studied by temperature variation Raman spectroscopy and PLTM.

The temperature variation Raman spectroscopy experiments showed evidence of a solid-solid transformation, starting at *ca.* 140 ºC, in which polymorph **2** convers into polymorph **1** (see Figure 12). In these experiments, a single crystal of polymorph **2** of AcROY was used as starting material, and a first spectrum was collected at 30 ºC. Then, the temperature was increased in steps of 10 ºC min^{-1}, and a spectrum was collected after each step from the initially probed sample spot. At 130 ºC, noticeable changes in the relative band intensities were started to be observed and at 140 ºC, the collected spectrum was different from the previous, indicating a phase transition. Comparing this spectrum with the ones collected for each polymorph (see Figure 5 and Table S2) it becomes clear that the observed phase transition corresponds to the conversion of polymorph **2** into polymorph **1**. However, at 140 ºC, Raman spectra obtained from other spots of the sample still rendered the characteristic spectrum of polymorph **2**, indicating that the observed solid-solid transition is slow and takes place in a relatively broad range of temperature. In order to better understand this event and, in particular, the range of temperatures in which it occurs, as well as to confirm the behaviour of polymorphs **1** and **3** studied by DSC analysis, a PLTM study of all polymorphs was undertaken. The results are shown in the PLTM video sent as Supporting Information (see also Figure S9).

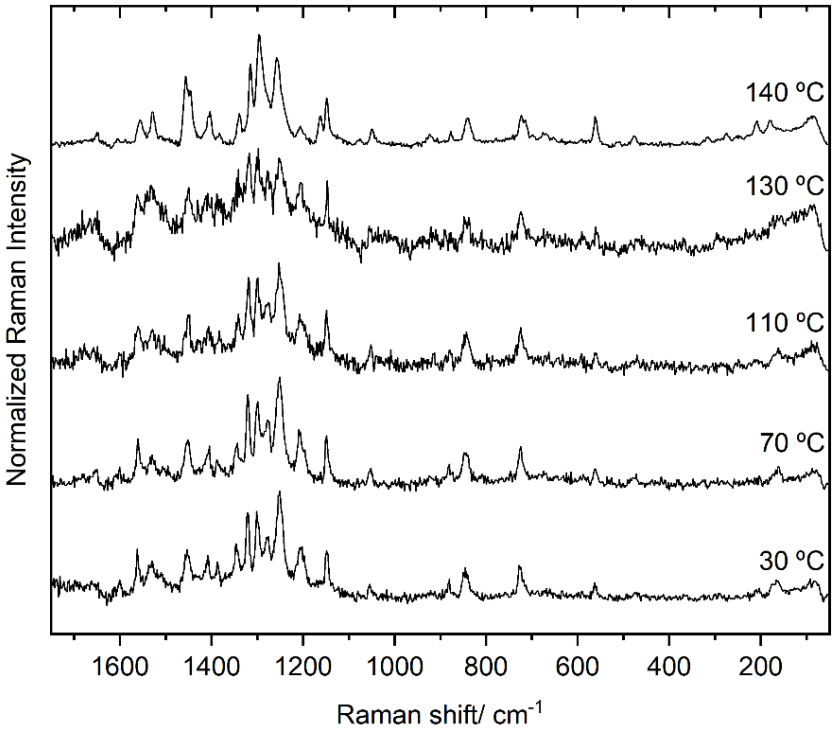

Figure 12 – Temperature variation Raman spectra obtained for a sample of polymorph **2** of AcROY (50-1750 cm^{-1} spectral region).

In the PLTM experiments (Figures S9 and PLTM video), temperature increase from 25 to 132 ºC did not lead to any visible changes in the sample (apart from the fact that some crystals moved out of the view area of the experiment due to air convection, as frequently seen in the type of experimental apparatus used). The rectangular shape crystal labelled as **2b** in Figure S9 was the first crystal of polymorph **2** to undergo the solid-solid transition to polymorph **1**, between *ca.* 144 and 145 ºC. The same transition was observed for crystal **2a** between 149 and 150 ºC (see Figure 13 and PLTM video) and, for crystal **2c** from 152 to 153 ºC, thus confirming that the **2** → **1** solid-solid transition occurs in a significantly wide range of temperature. The crystal marked as polymorph **3** in Figure S9 melts between 178 and 193 ºC, validating the DSC experiments for this polymorph. The non-labelled crystals in Figure S9 are crystals of polymorph **1**. Together with the crystals of polymorph **2** that first evolved into polymorph **1**, these crystals start to melt at *ca.* 195 ºC, the melting being complete at around 204 ºC, a result that is also in accordance with the obtained DSC data.

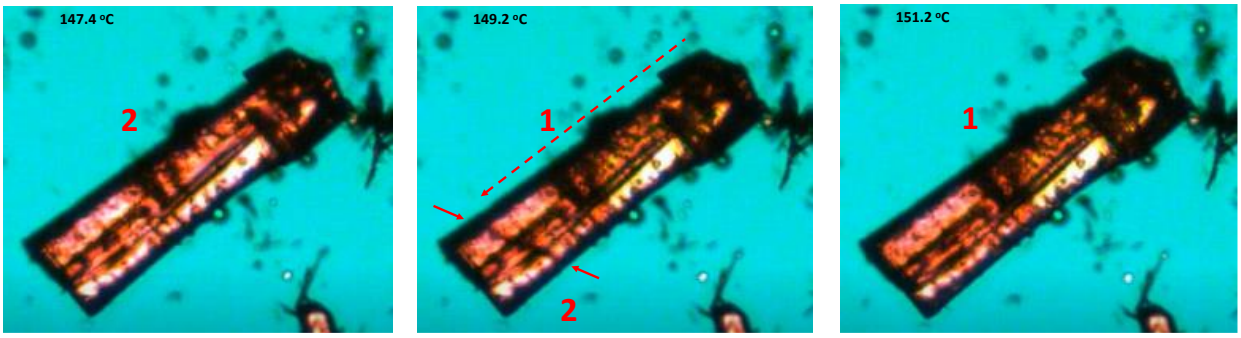

Figure 13 – PLTM images (3 consecutive frames extracted from the PLTM video submitted as Supporting Information) showing the **2** → **1** solid-solid transition for the crystal that in Figure S9 is labelled as 2a. In the middle frame, the transition is occurring. The solid arrows mark the front of the transition wave, while the dashed line indicate the direction of the transformation.

Conclusion

In this study, the synthesis and portrayal of the color polymorphism exhibited by the acetyl-derivative of ROY was undertaken. The structure and conformational landscape of the isolated molecule of the compound were investigated using DFT calculations. Four low-energy intramolecularly hydrogen-bonded conformers were located on the molecule's potential energy surface. The calculations revealed that the torsional potential of AcROY along θ is flat and allows easy interconversion between the conformers differing in the conformation around this coordinate (**A** and **B**, in one side, and **C** and **D**, in the other). The flatness of this potential also allows easy adjustment of the geometry of the molecule upon formation of a

crystal, when intermolecular interactions and packing also dictate the molecular conformations that better suits the energetic demands of a given crystalline phase.

The compound was found to exhibit color polymorphism, with 3 different polymorphs identified. The crystal structures of two of the polymorphs were solved by X-ray diffraction: polymorph **1** (burgundy) and polymorph **2** (orange). It was not possible to determine the crystal structure of the third polymorph (**3**, orange-yellowish), but the obtained powder X-ray diffraction, infrared and Raman spectroscopy, and DSC and PLTM data clearly demonstrate the existence of this additional polymorphic form. Indexation of its powder diffraction pattern showed that it is a monoclinic variety with lattice parameters a = 11.383(3) Å, b = 13.6609(3) Å, c = 25.247(7) Å, β =101.75(1), and exhibiting a more complex supramolecular structure compared to polymorphs **1** and **2** (most probably with belonging to the $P2_1/c$ space group, with Z = 4 and Z' = 3.

In the structurally characterized polymorphs (**1** and **2**), the AcROY molecules assume conformations corresponding to the lowest energy conformer predicted for the isolated molecule of the compound, slightly modified due to intermolecular forces and packing. These two polymorphs were found to be monotropically related, with polymorph **1** being the stable form and polymorph **3** the metastable crystal structure.

The dominant intermolecular interactions in polymorphs **1** and **2** were evaluated from the crystallographic structural data and also using Hirshfeld surface analysis, and were found to be significantly different: the contribution of the non-classical intermolecular hydrogen bonds of the CH···O type to the stabilization of the crystal structure of polymorph **1** is more important than for polymorph **2**, while the hydrogen bonds of the CH···N type play a more significant role in the stabilization of the crystal structure of polymorph **2** than in polymorph **1**. Another relevant structural different between the two polymorphs concerns the presence in polymorph **2** of short S···S contacts which are absent in polymorph **1**. Furthermore, while dispersive intermolecular interactions are important in both polymorphs, they are established between different fragments of the molecules in the two polymorphs. All these differences in the intermolecular interactions and packing influence the electronic properties of the AcROY molecules present in the crystals and, ultimately, determine their different colors, so that the observed polymorphism in AcROY is a case of packing-determined color polymorphism, somehow in contrast to ROY where the color polymorphism is mostly (but not exclusively, as mentioned in the Introduction) conformationally determined.[1-9]

Supporting Information

Figures S1-S9, with the ^{1}H and ^{13}C NMR spectra of AcROY, IR-ATR spectrum of the synthesized material, relative energy plot of the four conformers of AcROY showing the energy of the transition states for conformational isomerization, ORTEP plot depicting the anisotropic displacement ellipsoids, drawn at the 50% probability level, for polymorphs **1** and **2**, results of indexing of the powder diffractogram of

polymorph **3**, results of Hirshfeld analysis of these polymorphs, and PLTM images of the heating of the polymorphs; Tables S1-S3, with results of polymorph screening, assignment of the infrared and Raman spectra of the AcROY polymorphs, and selected valence angles in the molecules present in polymorphs **1** and **2** of AcROY; Crystallographic data Tables with the structural X-Ray data for polymorphs **1** and **2**; PLTM video. CIF files containing the supplementary crystallographic data were deposited at the Cambridge Crystallographic Data Centre, with references CCDC 2110241 (polymorph **1**) and 211242 (polymorph **2**).

Author Contributions

B.A.N. conceptualized the study, wrote a preliminary version of the manuscript and participated in most of the experimental work and in theoretical studies. M.C. worked on the polymorphs screening, and performed part of the DFT calculations and spectroscopic measurements. R.F. contributed to the conceptualization of the study and data curation, took responsibility for its supervision and wrote the final version of the manuscript; S.M.M.L. and T.M.V.D.P.M. were responsible for the development of the synthetic route and its implementation; M.E.S.E. participated in the design of the DSC studies and in the writing of the corresponding section of the manuscript; J.A.P. performed the XRD studies and wrote the corresponding section of the manuscript. All authors have participated in the discussion of the results and agreed with the final version of the manuscript.

Acknowledgements

The CQC-IMS is financially supported by the Portuguese Science Foundation ("Fundação para a Ciência e a Tecnologia" - FCT) – Projects CQC UIDB/00313/2020 and UIDP/00313/2020 (National Funds). CFisUC is funded by FCT through the projects UIDB/04564/2020 and UIDP/04564/2020. Access to instruments from Laser-Lab Coimbra and TAIL-UC (ICT_2009_02_012_1890) facilities funded under QREN-Mais Centro is gratefully acknowledged. We also acknowledge the UC-NMR facility for obtaining the NMR data (http://www.nmrccc.uc.pt). B.A.N. also acknowledges FCT for the SFRH/BD/129852/2017 PhD Scholarship.

References

1 X. Li, X. Ou, H. Rong, S. Huang, J. Nyman, L. Yu and M. Lu, , *Cryst. Growth Des.*, 2020, 20, 7093.

2 K. S. Gushurst, J. Nyman and S. X. M. Boerrigter, *CrystEngComm*, 2019, 21, 1363.

3 L. Yu, *Acc. Chem. Res.*, 2010, 43, 1257.

4 A. R. Tyler, R. Ragbirsingh, C. J. McMonagle, P. G. Waddell, S. E. Heaps, J. W. Steed, P. Thaw,

M. J. Hall and M. R. Probert, *Chem*, 2020, 6, 1755.

5 M. Tan, A. G. Shtukenberg, S. Zhu, W. Xu, E. Dooryhee, S. M. Nichols, M. D. Ward, B. Kahr and Q. Zhu, *Faraday Discuss.*, 2018, 211, 477.

6 A. Lévesque, T. Maris and J. D. Wuest, *J. Am. Chem. Soc.*, 2020, 142, 11873.

7 B. A. Nogueira, C. Castiglioni and R. Fausto, *Commun. Chem.*, 2020, 3, 1–12.

8 Z. Chen, Y. Gui, K. Cui, J. R. Schmit and L. Yu, *J. Phys. Chem. B*, 2021, 125, 10304.

9 L. R. Warren, E. McGowan, M. Renton, C. A. Morrison and N. P. Funnell, *Chem. Sci.*, 2021, 12, 12711.

10 B. A. Nogueira, S. M. M. Lopes, S. Lopes, T. Nikitin, A. C. B. Rodrigues, M. E. S. Eusébio, J. A. Paixão, T. M. V. D. Pinho e Melo, A. Milani, C. Castiglioni and R. Fausto, *Cryst. Growth Des.*, 2021, 21, 7269.

11 X. He, U. J. Griesser, J. G. Stowell, T. B. Borchardt and S. R. Byrn, *J. Pharm. Sci.*, 2001, 90, 371.

12 H. Li, J. G. Stowell, T. B. Borchardt and S. R. Byrn, *Cryst. Growth Des.*, 2006, 6, 2469.

13 H. Li, J. G. Stowell, X. He, K. R. Morris and S. R. Byrn, *J. Pharm. Sci.*, 2007, 96, 1079.

14 K. M. Lutker, Z. P. Tolstyka and A. J. Matzger, *Cryst. Growth Des.*, 2008, 8, 136.

15 G. M. Sheldrick, *Acta Crystallogr., Sect. C: Struct. Chem.*, 2015, 71, 3.

16 G. M. Sheldrick, *Acta Crystallogr., Sect. A*, 2015, 71, 3.

17 A. L. Spek, *J. Appl. Cryst.*, 2003, 36, 7.

18 A. A. Coelho, *J. Appl. Crystallogr.*, 2017, 50, 1.

19 A. A. Coelho, *J. Appl. Crystallogr.*, 2018, 51, 210.

20 Frisch, M. J.; Trucks, G. W.; Schlegel, H. B.; Scuseria, G. E.; Robb, M. A.; Cheeseman, J. R.; Scalmani, G.; Barone, V.; Mennucci, B.; Petersson, G. A. *et al.* Gaussian 09 (Revision D.01) Gaussian, Inc. Wallingford (CT, USA), 2009.

21 A. D. Becke, *Phys. Rev. A*, 1988, 38, 3098.

22 C. Lee, W. Yang and R. G. Parr, *Phys. Rev. B*, 1988, 37, 785.

23 A. D. McLean and G. S. Chandler, *J. Chem. Phys.*, 1980, 72, 5639.

24 S. K. Wolff, D. J. Grimwood, J. J. McKinnon, M. J. Turner, D Jayatilaka, and M. A. Spackman, Crystal Explorer17 (version 17.5), University of Western Australia, Crawley (AUS), 2017.

25 J. J. McKinnon, A. S. Mitchell and M. A. Spackman, *Chem. Eur. J.*, 1998, 4, 2136.

26 M. A. Spackman and J. J. McKinnon, *CrystEngComm*, 2002, 4, 378.

27 A. Parkin, G. Barr, W. Dong, C. J. Gilmore, D. Jayatilaka, J. J. McKinnon, M. A. Spackman and C. C. Wilson, *CrystEngComm*, 2007, 9, 648.

28 A. L. Rohl, M. Moret, W. Kaminsky, K. Claborn, J. J. McKinnon and B. Kahr, *Cryst. Growth Des.*, 2008, 8, 4517.

29 M. A. Spackman and D. Jayatilaka, *CrystEngComm*, 2009, 11, 19.

30 K. J. Thorley and I. McCulloch, *J. Mater. Chem. C*, 2018, 6, 12413.

31 Y. Nagao, T. Hirata, S. Goto, S. Sano, A. Kakehi, K. Iizuka and M. Shiro, *J. Am. Chem. Soc*., 1998, 120, 3104.

32 L. I. L. Cabral, E. M. Brás, M. S. C. Henriques, C. Marques, L. Frija, L. Barreira, J. A. Paixão, R. Fausto and M. L. S. Cristiano, *Chem. Eur. J.*, 2018, 24, 3251.

33 S. Tang, A. Yusov, Y. Li, M. Tan, Y. Hao, Z. Li, Y.-S. Chen, C. T. Hu, B. Kahr and M. D. Ward, *Mater. Chem. Front.*, 2020, 4, 2378.

34 S. P. Thomas and M. A. Spackman, *Austr. J. Chem.*, 2018, 71, 279.

35 J. Nyman, L. Yu and S. M. Reutzel-Edens, *CrystEngComm*, 2019, 21, 2080.

36 S. Chen, I. A. Guzei, and L. Yu, *J. Am. Chem. Soc.*, 2005, 127, 9881.

37 M. A. Spackman and P. G. Byrom, *Chem. Phys. Lett.*, 1997, 267, 215.

38 A. Burger and R. Ramberger, *Microchim. Acta*, 1979, 72, 259.

39 A. Burger and R. Ramberger, *Microchim. Acta*, 1978, 72, 273.

40 L. Yu, *J. Pharm. Sci.*, 1995, 84, 966.

Table of Contents Graph

For

Portrayal of the Color Polymorphism in the 5-Acetyl-derivative of ROY

Bernardo A. Nogueira,[*,1] Maria Carvalho,[1] José A. Paixão,[2] M. Ermelinda S. Eusébio,[1]

Susana M. M. Lopes,[1] Teresa M. V. D. Pinho e Melo[1] and Rui Fausto[1]

[1] *University of Coimbra, CQC-IMS, Department of Chemistry, P-3004-535 Coimbra, Portugal.*
[2] *University of Coimbra, CFisUC, Department of Physics, P-3004-516 Coimbra, Portugal.*

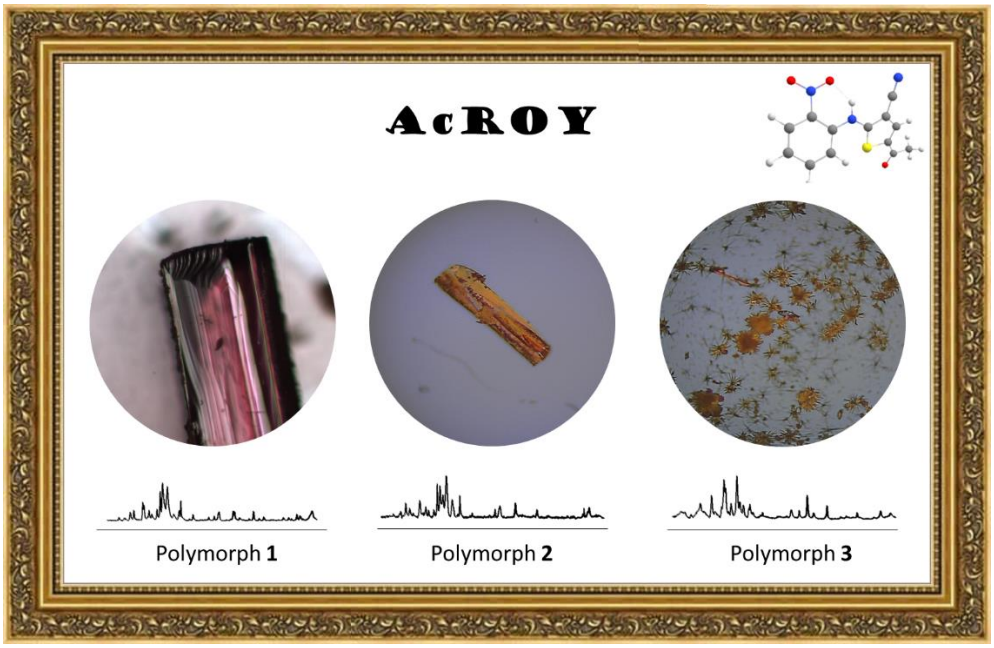

* Corresponding author e-mail: ban@qui.uc.pt